

◇ MONOGRAPH EXCERPT ◇

MATTER ANTIMATTER FLUCTUATIONS

SEARCH, DISCOVERY AND ANALYSIS OF B_s FLAVOR OSCILLATIONS

NUNO LEONARDO

Complete work published as:

Analysis of B_s oscillations at CDF, MIT Thesis (2006)

Matter antimatter fluctuations, Monograph, LAP Lambert (2011)

Author © Nuno Teotónio Leonardo

2.2 Phenomenology of flavor oscillations

The quarks, along with the leptons (electron e , muon μ , tau τ , and associated neutrinos), constitute the known building blocks of matter. They appear as six *quark-flavors*: the so-called up-type (u, c, t) and down-type (d, s, b) quarks have electric charges $+\frac{2}{3}e$ and $-\frac{1}{3}e$, respectively (e being the magnitude of the electron's charge); the associated antiparticles have symmetric charges. The quark masses [1] (computed in a common renormalization scheme) present the following observed hierarchy

| | | |
|--------------------------|------------------------------|--------------------------------|
| u (up) | c (charm) | t (top) |
| 1.5-4 MeV/c ² | 1.15-1.35 GeV/c ² | (174.3±5.1) GeV/c ² |
| d (down) | s (strange) | b (bottom) |
| 4-8 MeV/c ² | 80-130 MeV/c ² | 4.1-4.4 GeV/c ² |

which is not understood, lacking an experimentally established, fundamental theory of masses.

Transitions take place between the up-type and down-type quarks, with relative strengths which may be represented in a matrix of the form

$$\begin{pmatrix} V_{ud} & V_{us} & V_{ub} \\ V_{cd} & V_{cs} & V_{cb} \\ V_{td} & V_{ts} & V_{tb} \end{pmatrix}.$$

Within the SM, such quark-flavor changing transitions are accomplished by the weak interactions, and the quark mixing matrix above is *unitary* and referred to as the CKM matrix. Flavor changing neutral currents (FCNC) corresponding to transitions among the up-type quarks or the down-type quarks are, at lowest level in perturbation theory, absent. The CKM elements correspond to fundamental parameters not predicted by the theory; they must be extracted from data.

Unlike leptons, quarks are not observed as physical particles, rather they are confined inside hadrons. Among these, the neutral B meson systems are of central importance for the phenomena we set out to study. These meson states are formed of a bottom (anti-) quark together with either a down or a strange quark,

$$B^0(\bar{b}d), \bar{B}^0(b\bar{d}) \quad \text{and} \quad B_s(\bar{b}s), \bar{B}_s(b\bar{s}).$$

The aforementioned quark-flavor changing interactions induce transitions among the neutral B and \bar{B} states, for both the B^0 and B_s meson systems. By means of those (weak) interactions, the effective Hamiltonian describing the two-state system acquires off-diagonal contributions, such that the system's mass eigenstates differ from those states of definite

quark-flavor. As a result, time-dependent transitions develop between the B and \bar{B} states. These transitions are referred to as B meson *mixing* or *flavor oscillations*, and occur with a frequency determined by the difference Δm between the two mass eigenvalues of the system, as derived in Section 2.1.

By performing measurements of processes governed by the above mentioned weak transitions one is in principle able to obtain information about the underlying parameters of the theory, V_{ij} . In particular, the measurement of the oscillation frequencies of the B^0 and B_s systems, denoted respectively Δm_d and Δm_s , provides a determination of the moduli of the matrix elements V_{td} and V_{ts} . Such determinations in general suffer, nevertheless, from complications stemming from the fact that the quarks are confined in hadrons, and associated theoretical uncertainties enter into the interpretation of the measurements. These uncertainties in the case of the B^0 and B_s mixing systems are considerably large. As may be expected, however, since these mesons differ only by their light quarks, a significant uncertainty reduction is obtained for the ratio of the oscillation frequencies of the two systems. As a result, a precise determination of the ratio of the CKM elements $|V_{td}/V_{ts}|$ is possible.

Various other processes are sensitive to the different matrix elements. These involve weak decays and asymmetries, not necessarily restricted to B meson systems. Such measurements along with B mixing translate into constraints on the elements of the CKM matrix, and together are used to test its unitarity and the standard flavor description. Furthermore, B mixing, which occurs in the SM only at loop level, is expected to be particularly sensitive to new physics sources.

Next we further discuss the CKM ansatz, the origin and parameterization of the quark mixing matrix, and how measurements of flavor oscillations may be employed to constrain the underlying flavor model.

2.2.1 Quark masses and flavor changing interactions

Quark masses

The mass term in the Lagrangian density for a Dirac spinor field $\psi(x)$ is of the form

$$- m \bar{\psi} \psi \quad (2.26)$$

where m is the fermion mass, and $\bar{\psi}$ is the adjoint field ($\bar{\psi} \equiv \psi^\dagger \gamma^0$; γ^μ will refer to a consistent set of Dirac matrices [2]). Expanded in terms of the left and right chirality projections ($\psi_{R,L} \equiv \frac{1 \pm \gamma^5}{2} \psi$), (2.26) may be written as: $-m(\bar{\psi}_L \psi_R + \bar{\psi}_R \psi_L)$.

The mass terms for the quark fields may, correspondingly, be in general expressed as

$$\mathcal{L}_M = -\bar{\mathbf{u}}_R^{\circ T} \mathbf{m}_u \mathbf{u}_L^\circ - \bar{\mathbf{d}}_R^{\circ T} \mathbf{m}_d \mathbf{d}_L^\circ + \text{h.c.} . \quad (2.27)$$

The up-type and down-type quark fields are contained in the column vectors \mathbf{u}° and \mathbf{d}° , respectively (with dimension given by the number of families); “h.c.” stands for the hermitian conjugate counterparts of the terms shown. The mass matrices \mathbf{m}_u and \mathbf{m}_d are, for generality, complex-valued and non-diagonal. The Lagrangian (2.27) should be regarded in a more general context as effectively obtained from a fundamental theory of masses.

Fermionic mass terms, as in (2.26) and (2.27), are not invariant under gauge transformations, where the right- and left-handed fields may belong to different representations of the gauge group. They cannot thus appear in the bare Lagrangian of such gauge invariant theories, and are instead effectively generated in general through spontaneous symmetry breaking. In the SM electroweak theory, the $SU(2) \otimes U(1)$ local symmetry spontaneous breakdown is achieved by introducing a scalar field with non-vanishing vacuum-expectation-value (vev). The scalar field is realized by the Higgs boson, and the mentioned mechanism thereby gives mass to gauge bosons, charged leptons, and quarks. Specifically, the fermion masses arise from Yukawa terms, coupling the Higgs and the fermion fields,

$$-Y\bar{\psi}\psi\phi \xrightarrow[\text{symmetry breaking}]{\text{spontaneous}} -Y\bar{\psi}\psi(v + \phi'), \quad (2.28)$$

where Y is the Yukawa coupling with the Higgs field $\phi(x)$, and v and $\phi'(x)$ are respectively its vev and excitation above background. The quark mass terms in (2.27) are then given by

$$\mathbf{m}_f = v\mathbf{Y}_f \quad (f = u, d), \quad (2.29)$$

with $(\mathbf{Y}_f)_{ij}$ representing the associated Yukawa couplings. The origin of these couplings and their apparent hierarchy are not understood. The Higgs scalar field in the SM consists of a single doublet of the gauge group; and ϕ above in (2.28) corresponds more precisely to the scalar component not eaten up by gauge symmetry. The quark mass matrices however could potentially arise from a more elaborate Higgs sector, leaving behind a more complicated set of quark-Higgs couplings, with possibly multiple vev 's. The general algebraic construction (of the CKM ansatz) that follows would hold equally well in such scenarios.

The mass matrices, \mathbf{m}_u and \mathbf{m}_d , may be diagonalized with the help of two unitary matrices each – L_u, R_u and L_d, R_d – as

$$L_u\mathbf{m}_uR_u^\dagger = \hat{\mathbf{m}}_u, \quad L_d\mathbf{m}_dR_d^\dagger = \hat{\mathbf{m}}_d, \quad (2.30)$$

where $\hat{\mathbf{m}}_u$ and $\hat{\mathbf{m}}_d$ are diagonal, with real, positive eigenvalues, corresponding to the individual quark masses,

$$\hat{\mathbf{m}}_{u(d)} = \text{diag} (m_{u(d)}, m_{c(s)}, m_{t(b)}) . \quad (2.31)$$

The quark fields in (2.27) are accordingly translated into their mass eigenstates, denoted \mathbf{u} and \mathbf{d} , through the unitary transformations specified by (2.30),

$$\mathbf{u}_L = L_u \mathbf{u}_L^\circ, \quad \mathbf{u}_R = R_u \mathbf{u}_R^\circ, \quad \mathbf{d}_L = L_d \mathbf{d}_L^\circ, \quad \mathbf{d}_R = R_d \mathbf{d}_R^\circ. \quad (2.32)$$

Although the underlying (electroweak) theory is first written down in terms of the gauge basis states, actual calculations which confront theory with experiment are performed using the mass basis states.

Flavor changing interactions

The SM weak interactions induce flavor changing transitions through charged currents coupling to the W^\pm bosons. For the quark fields, represented by the original field arrays \mathbf{u}° and \mathbf{d}° , these flavor changing interactions are described by

$$\mathcal{L}_W = \frac{g}{\sqrt{2}} \bar{\mathbf{u}}_L^{\circ T} \gamma^\mu \mathbf{d}_L^\circ W_\mu^+ + \text{h.c.}, \quad (2.33)$$

where g denotes the $SU(2)$ gauge coupling constant. Once the quark fields are expressed in the mass eigenstates basis, via the transformations (2.32), the above expression becomes

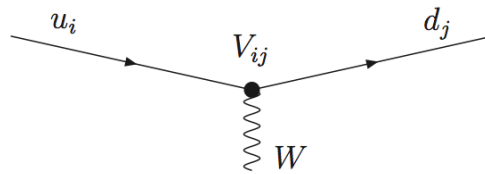
$$\mathcal{L}_W = \frac{g}{2\sqrt{2}} \bar{\mathbf{u}}^T \gamma^\mu (1 - \gamma^5) \mathbf{V} \mathbf{d} W_\mu^+ + \text{h.c.} \quad (2.34)$$

with

$$\mathbf{V} \equiv L_u L_d^\dagger. \quad (2.35)$$

The unitary quark-mixing matrix \mathbf{V} is referred to as the Cabibbo-Kobayashi-Maskawa (CKM) matrix [4, 5].

The charged current interactions of (2.34) produce transitions between up- and down-type quarks, which occur across the various quark families, with amplitudes determined by the corresponding CKM matrix elements. This may be represented by the diagram



The b quark decays to a c or u quark and a virtual W boson, with couplings given by the V_{cb} or V_{ub} matrix elements, respectively. The dominant, tree-level diagrams describing

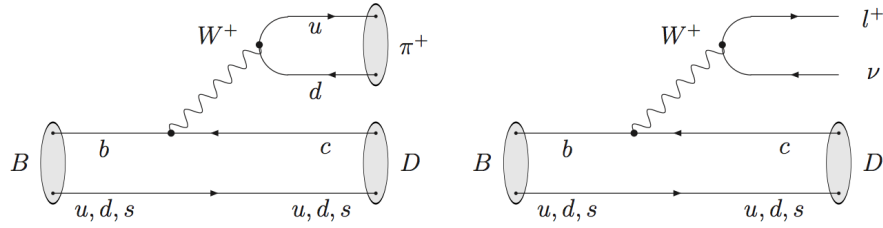


Figure 2.1: Tree-level Feynman diagrams describing B meson decays: $B \rightarrow D\pi^+$ (*hadronic*) and $B \rightarrow Dl^+\nu$ (*semileptonic*).

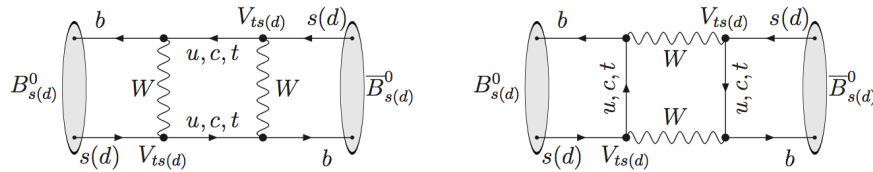


Figure 2.2: Leading Feynman diagrams contributing to B_s and B^0 flavor oscillations.

the decays of B mesons are correspondingly represented in Figure 2.1. In case the W boson exchange occurs with a (u_i, \bar{d}_j) quark pair or a (l^+, ν) lepton pair, the B decay is in general also named *hadronic* or *semileptonic*, respectively.

The weak charged current interactions of (2.34) are further capable, at loop level, of inducing B to \bar{B} transitions in the neutral B meson systems. These transitions are represented in Figure 2.2, and will be addressed below.

2.2.2 CKM ansatz and the unitarity triangle

We have seen above that the quark mass eigenstates, \mathbf{u} and \mathbf{d} , differ in general from the quark field combinations which belong to the gauge group representations of the underlying theory. The states which participate in the transitions of the charged weak current are linear combinations of the mass eigenstates. By convention, the mixing is assigned to the down-type quarks, being expressed by the CKM matrix (2.35) as

$$\mathbf{d}' = \mathbf{V} \mathbf{d}, \quad (2.36)$$

or, in an expanded form,

$$\begin{pmatrix} d' \\ s' \\ b' \end{pmatrix} = \begin{pmatrix} V_{ud} & V_{us} & V_{ub} \\ V_{cd} & V_{cs} & V_{cb} \\ V_{td} & V_{ts} & V_{tb} \end{pmatrix} \begin{pmatrix} d \\ s \\ b \end{pmatrix}. \quad (2.37)$$

The SM does not predict the content of the CKM matrix \mathbf{V} , rather, its matrix elements must be phenomenologically extracted from data.

We note in passing that the experimentally constrained observables, the CKM matrix and the mass matrices eigenvalues, are insufficient for reconstructing the full mass matrices (2.30). The latter requires knowledge of both left and right handed rotation matrices, $L_{u(d)}$ and $R_{u(d)}$. This is the starting difficulty one encounters in trying to construct a theory of masses. Such models proceed through theoretically motivated hypotheses which ought to be tested via predicted relations among the observables.

CKM matrix parameterization

The quark mixing matrix \mathbf{V} , being the product of unitary matrices (2.35), is itself unitary. A general 3×3 unitary matrix has 9 parameters. Among these, three are rotation angles; this is the number of parameters of a $O(3)$ rotation, *e.g.* the Euler angles. The remaining 6 parameters are phases. Some of these can be absorbed by making phase rotations of the quark fields; noticing that an overall phase, common to all six quark fields is redundant, we deduce that only 5 of these phases can be removed. This may be written explicitly as

$$\mathbf{V} \mapsto P(\sigma_1, \sigma_2, \sigma_3) \mathbf{V} P(0, \sigma_4, \sigma_5), \quad (2.38)$$

with $P(\sigma_i, \sigma_j, \sigma_k) \equiv \text{diag}(e^{i\sigma_i}, e^{i\sigma_j}, e^{i\sigma_k})$. Once the phases σ_i are absorbed into the redefinition of the quark fields, \mathbf{V} finally contains 4 real parameters: 3 angles and 1 phase.

There are many ways to parameterize the CKM matrix in terms of four independent parameters. The numerical value of the physical phase, for instance, is not unique due to the arbitrariness in the choice of the unphysical phases, thus varying with the adopted parameterization. The standard CKM parameterization [6] is constructed as the product of three rotation matrices R_{ij} characterized by the Euler angles θ_{12} , θ_{23} , θ_{13} along with a phase δ ,

$$\begin{aligned} \mathbf{V} &= R_{23} P(-\delta, 0, 0) R_{13} P(\delta, 0, 0) R_{12} \\ &= \begin{pmatrix} 1 & 0 & 0 \\ 0 & c_{23} & s_{23} \\ 0 & -s_{23} & c_{23} \end{pmatrix} \begin{pmatrix} c_{13} & 0 & s_{13} e^{-i\delta} \\ 0 & 1 & 0 \\ -s_{13} e^{i\delta} & 0 & c_{13} \end{pmatrix} \begin{pmatrix} c_{12} & s_{12} & 0 \\ -s_{12} & c_{12} & 0 \\ 0 & 0 & 1 \end{pmatrix} \\ &= \begin{pmatrix} c_{13} c_{12} & s_{12} c_{13} & s_{13} e^{-i\delta} \\ -s_{12} c_{23} - s_{23} s_{13} c_{12} e^{i\delta} & c_{23} c_{12} - s_{23} s_{13} s_{12} e^{i\delta} & s_{23} c_{13} \\ s_{23} s_{12} - s_{13} c_{23} c_{12} e^{i\delta} & -s_{23} c_{12} - s_{13} s_{12} c_{23} e^{i\delta} & c_{23} c_{13} \end{pmatrix}. \end{aligned} \quad (2.39)$$

The mixing angles θ_{ij} (for generation labels $i, j = 1, 2, 3$) can all be chosen to lie in the first

quadrant, such that $c_{ij} \equiv \cos \theta_{ij}$ and $s_{ij} \equiv \sin \theta_{ij}$ are positive quantities, while the phase δ may vary between 0 and 2π .

Following the observation of a hierarchy between the mixing angles, $s_{13} \ll s_{23} \ll s_{12} \ll 1$, an expansion was proposed by Wolfenstein [7] in terms of powers of $\lambda = s_{12}$ (*i.e.* the sine of θ_{12} , which is identified with the Cabibbo angle), along with parameters A , ρ and η intended to be of order unity. We adopt here a generalization [8] where the real parameters A , λ , ρ and η are *defined* (to all orders) through the following relations,

$$s_{12} = \lambda, \quad s_{23} = A\lambda^2, \quad s_{13}e^{i\delta_{13}} = A\lambda^3(\rho + i\eta). \quad (2.40)$$

Making this change of variables in the standard parameterization (2.39), we obtain the CKM matrix as a function of (A, λ, ρ, η) which satisfies unitarity exactly. We may next perform an expansion in powers of λ , to obtain

$$\mathbf{V} = \begin{pmatrix} 1 - \frac{\lambda^2}{2} - \frac{\lambda^4}{8} & \lambda & A\lambda^3(\rho - i\eta) \\ -\lambda + A^2\lambda^5\left(\frac{1}{2} - \rho - i\eta\right) & 1 - \frac{\lambda^2}{2} - \frac{1}{8}\lambda^4(1 + 4A^2) & A\lambda^2 \\ A\lambda^3\left(1 - (\rho + i\eta)\left(1 - \frac{\lambda^2}{2}\right)\right) & -A\lambda^2 + A\lambda^4\left(\frac{1}{2} - \rho - i\eta\right) & 1 - \frac{1}{2}A^2\lambda^4 \end{pmatrix} + \mathcal{O}(\lambda^6). \quad (2.41)$$

This explicitly illustrates the observed hierarchy in the magnitude of the CKM elements: the on-diagonal elements are large, of order unity, while the off-diagonal entries are smaller, indicating the relative suppression of cross-generation transitions. For example, $b \rightarrow c$ transitions are suppressed by λ^2 and $b \rightarrow u$ transitions are suppressed by λ^3 . Truncated expansions in λ are instructive, as for such illustrative purposes; however we find otherwise no need here to make such approximations.

Physically meaningful quantities are, of course, independent of the adopted parameterization. Phase-convention invariant quantities include the moduli, $|V_{ij}|$, of the matrix elements. The parameters $\lambda = |V_{us}|/\sqrt{|V_{ud}|^2 + |V_{us}|^2}$ and $A = |V_{cb}/V_{us}|/\lambda$ are thus phase invariant, while ρ and η , with $\rho + i\eta = V_{ub}^*/(A\lambda^3)$, are not.

CP violation

Irreducible phases in the quark mixing matrix, which imply the presence of weak complex couplings, lead to violation of the charge-parity CP symmetry [10, 9]. If the Hamiltonian is complex then the theory is not invariant under time reversal, $THT^{-1} \neq H$, due to the complex conjugation produced by the T operation. The combined operation CPT is a basic symmetry of any (local Poincaré invariant) quantum field theory; it follows that non-conservation of T implies that CP must be violated as well.

As we have seen, in the case of three quark generations there is one such single phase. The generalization to the case of n generations contains $(n-1)(n-2)/2$ phases along with $n(n-1)/2$ angles. For less than 3 generations no physical phase would remain, which makes the third quark generation a requirement for the existence of CP violation in the quark sector. This also means that the phase of the CKM matrix can have physical consequences only in processes involving all three generations, which typically corresponds to processes containing weak interaction loop contributions.

A phase-convention independent measure of CP violation in the SM quark sector is given by

$$\begin{aligned} \text{Im det} \left([\mathbf{m}_u \mathbf{m}_u^\dagger, \mathbf{m}_d \mathbf{m}_d^\dagger] \right) &= 2 J (m_t^2 - m_c^2)(m_t^2 - m_u^2)(m_c^2 - m_u^2) \\ &\times (m_b^2 - m_s^2)(m_b^2 - m_d^2)(m_s^2 - m_d^2) . \end{aligned} \quad (2.42)$$

The Jarlskog invariant [11], J , contains the dependence on the CKM elements, and has the general representation

$$\text{Im} (V_{ij} V_{kl} V_{il}^* V_{kj}^*) = J \sum_{m,n=1}^3 \epsilon_{ikm} \epsilon_{jln} \quad (2.43)$$

which in terms of the standard (2.39) and generalized Wolfenstein (2.41) parameterizations is given by

$$J = c_{12} c_{23} c_{13}^2 s_{12} s_{23} s_{13} \sin \delta = A^2 \lambda^6 \eta (1 - \lambda^2/2) + \mathcal{O}(\lambda^{10}) . \quad (2.44)$$

The requirements for CP violation include therefore the non-degeneracy of the up-type and down-type quark masses, and the non-vanishing of the CKM phase, hence $J \neq 0$. Both conditions are experimentally verified.

Unitarity triangle

The unitarity of the CKM matrix leads to various relations among its elements, which may be expressed in terms of geometric representations. The unitarity conditions are summarized as

$$\sum_i V_{ij} V_{ik}^* = \delta_{jk} = \sum_i V_{ji} V_{ki}^* . \quad (2.45)$$

For example, from the orthogonality of the first and third columns, one has

$$V_{ud} V_{ub}^* + V_{cd} V_{cb}^* + V_{td} V_{tb}^* = 0 . \quad (2.46)$$

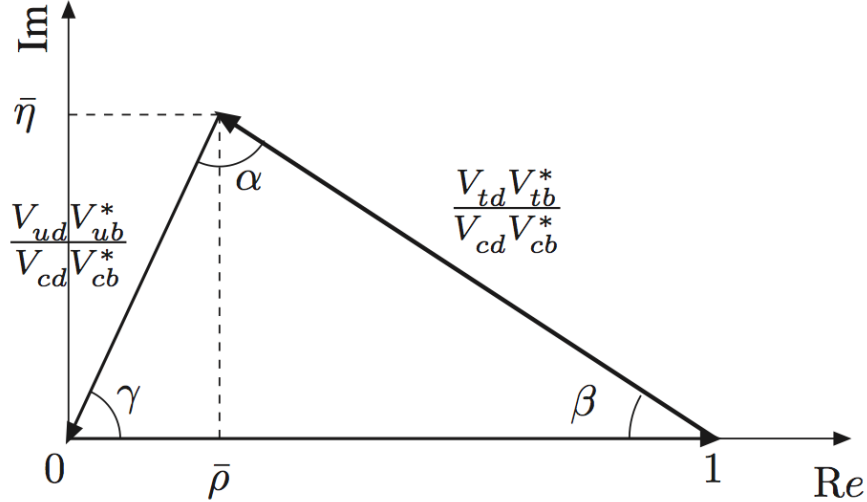


Figure 2.3: The unitarity triangle in the complex plane.

This relation requires the sum of three complex quantities to vanish, and can thus be represented in the complex plane as a triangle [12]. Phase transformations lead to rotations of the triangle in the complex plane. The angles and the sides of the triangle, which are given by the moduli of the matrix elements, are phase-convention independent and constitute physical observables. Overall, (2.45) defines six triangles corresponding to orthogonality relations. All such triangles have a common area, identical to $|J|/2$.

The geometric representation of the unitarity relation (2.46) is named the *unitarity triangle* (UT). The UT is customarily re-scaled such that one of the sides has unit length and is aligned with the real axis. This is represented in Figure 2.3. The re-scaling factor is chosen to be the inverse of $V_{cd}V_{cb}^*$, emphasizing the less well determined parameters (ρ, η) . The apex of the UT is given by the following phase-convention independent definition

$$\bar{\rho} + i\bar{\eta} \equiv -\frac{V_{ud}V_{ub}^*}{V_{cd}V_{cb}^*}. \quad (2.47)$$

Expressed in terms of the parameterization (2.41), one finds

$$\rho + i\eta = \frac{\sqrt{1 - A^2\lambda^4}(\bar{\rho} + i\bar{\eta})}{\sqrt{1 - \lambda^2}[1 - A^2\lambda^4(\bar{\rho} + i\bar{\eta})]}, \quad (2.48)$$

which is valid to all orders in λ ; to leading order, $\bar{\rho}$ and $\bar{\eta}$ are given by

$$\bar{\rho} = \rho(1 - \lambda^2/2) + \mathcal{O}(\lambda^4), \quad \bar{\eta} = \eta(1 - \lambda^2/2) + \mathcal{O}(\lambda^4). \quad (2.49)$$

The UT has the characteristic that all sides are of comparable size, of order λ^3 in the parameterization (2.41). This reveals convenient from an experimental point of view, if all angles

and sides are to be precisely constrained. The sides of the UT (besides that along the real axis which is normalized to unity) read to all orders

$$R_u \equiv \left| \frac{V_{ud}V_{ub}^*}{V_{cd}V_{cb}^*} \right| = \sqrt{\bar{\rho}^2 + \bar{\eta}^2}, \quad (2.50)$$

$$R_t \equiv \left| \frac{V_{td}V_{tb}^*}{V_{cd}V_{cb}^*} \right| = \sqrt{(1 - \bar{\rho})^2 + \bar{\eta}^2}. \quad (2.51)$$

The angles are defined as

$$\alpha = \arg \left(-\frac{V_{td}V_{tb}^*}{V_{ud}V_{ub}^*} \right), \quad \beta = \arg \left(-\frac{V_{cd}V_{cb}^*}{V_{td}V_{tb}^*} \right), \quad \gamma = \arg \left(-\frac{V_{ud}V_{ub}^*}{V_{cd}V_{cb}^*} \right), \quad (2.52)$$

and may be expressed, again to all orders in λ , as

$$\begin{aligned} \cos \gamma &= \bar{\rho}/R_u, & \sin \gamma &= \bar{\eta}/R_u, \\ \cos \beta &= (1 - \bar{\rho})/R_t, & \sin \beta &= \bar{\eta}/R_t, \\ \alpha &= \pi - \beta - \gamma. \end{aligned} \quad (2.53)$$

The CKM phase in the parameterization (2.39) reads $\delta = \gamma + A^2\lambda^4\eta + \mathcal{O}(\lambda^6)$.

The sides and the angles of the UT may all be experimentally determined. By doing so, one can over-constrain the shape of the triangle, testing the unitarity of the CKM matrix. As we shall see next, the measurement of flavor oscillations in both neutral B meson systems will provide a stringent constraint in one side, R_t , of the UT.

We also like to mention that in the future the copious production of B_s mesons — at the Tevatron, the LHC and $\Upsilon(5S)$ resonance machines — will allow further exploration of the unitarity triangle (UT_s) which results from the orthogonality of the second and third columns of the CKM matrix. In this other triangle not all sides are of similar sizes. The smallest side corresponds to $V_{us}V_{ub}^*/V_{cs}V_{cb}^*$, and has a relative magnitude of the order of λ^2 ; the small angle opposing this side is given by

$$\beta_s = \arg \left(-\frac{V_{ts}V_{tb}^*}{V_{cs}V_{cb}^*} \right). \quad (2.54)$$

The determination of this phase, accessible for example through the study of the CP asymmetry in B_s decays into final CP eigenstates such as $J/\psi\phi$, is complementary to the Δm_s measurement which itself corresponds to the modulo of the mixing process amplitude (2.20).

2.3 Standard model and beyond

2.3.1 Model constraining

Provided that the CKM matrix elements govern the flavor changing processes, one may be able to use experimental inputs such as measurements of decay rates, asymmetries, and

mixing to constrain the matrix parameters. In particular, the unitarity of the CKM matrix is in this way tested, validating the three-generation SM, while any discrepancies found will provide insight on sources of new physics.

The connection between the properties of the b -flavored hadrons, which are what is experimentally detected, and the underlying quark dynamics is achieved employing effective field theory techniques. These proceed by separating the different energy scales involved, such that the high scale phenomena associated to the flavor structure may be treated separately from the complications of non-perturbative hadronic physics. The interactions at higher scales, basically, give rise to local operators at lower scales. An effective weak Hamiltonian describing the flavor changing processes is obtained through an operator product expansion [2]. The hadronic matrix elements are tackled by techniques such as heavy quark effective theory and lattice QCD. The most notable application of lattice QCD, in the context of CKM parameter determination, is in effect to mixing related quantities; uncertainties in those quantities are currently dominant in CKM fits.

The leading, lowest order diagrams that contribute to the $B_q^0 \bar{B}_q^0$ ($q = d, s$) transitions are shown in Figure 2.2. They correspond to four-vertex “box” graphs containing two W and two up-type quark internal lines. The dominant fermion contribution in the loop is provided by the t quark; the contributions from the lighter quarks are suppressed by $(m_{u,c}/m_W)^2$. The effective coupling therefore becomes proportional to $(V_{tb}^* V_{td})^2$ and $(V_{tb}^* V_{ts})^2$, respectively, for the B^0 and B_s systems. Correspondingly, the following relation may be written for the oscillation frequencies,

$$\Delta m_q = C_q |V_{tb}^* V_{tq}|^2, \quad (q = d, s). \quad (2.55)$$

The coefficients C_q are evaluated in the framework of the effective theory, the full expression being given in (12.15); the derivation is outlined in Section 2.1. In principle, and further noting that $V_{tb} \approx 1$, the relations (2.55) may be used to constrain the individual CKM matrix elements $|V_{td}|$ and $|V_{ts}|$ from the measurements of Δm_d and Δm_s . The power of these constraints nevertheless is hampered by the systematic uncertainties which characterize the lattice calculation of the hadronic matrix elements, which are contained in C_q . Several of these uncertainties cancel out once the ratio of the oscillation frequencies of the two systems is formed,

$$\frac{\Delta m_d}{\Delta m_s} = \frac{C_d |V_{td}|^2}{C_s |V_{ts}|^2} = \frac{m_{B^0}}{m_{B_s}} \xi_\Delta^{-2} \frac{|V_{td}|^2}{|V_{ts}|^2}. \quad (2.56)$$

Here the parameter ξ_Δ quantifies the SU(3) flavor symmetry breaking corrections to the matrix elements, and can be calculated more accurately in lattice QCD than the matrix

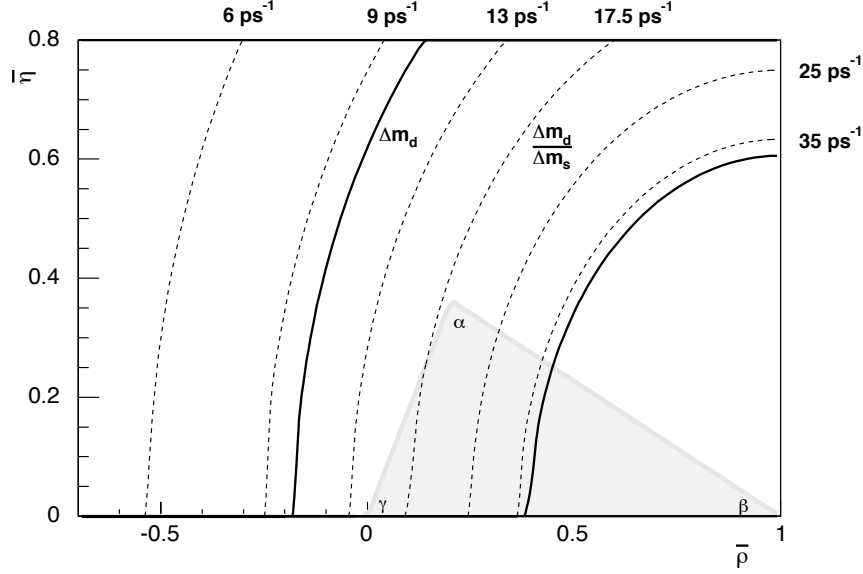


Figure 2.4: Constraints on the apex of the unitarity triangle from B mixing measurements; the continuous lines indicate the Δm_d allowed region (95% CL), while the dashed lines project a set of Δm_s values.

elements themselves. (Currently, while uncertainties on the computations of C_q are of the order of 15%, a precision of better than 4% is attained in the computation of ξ_Δ [13].)

The constraints on the CKM matrix elements are translated into probability regions in the space of its parameters (2.41), and in particular may be used to constrict the apex of the UT. For the B^0 system, (2.55) approximately describes a circle around $(1, 0)$ in the $(\bar{\rho}, \bar{\eta})$ plane,

$$\Delta m_d = C_d \lambda^6 A^2 [(1 - \bar{\rho})^2 + \bar{\eta}^2], \quad (2.57)$$

to which a distortion appears at $\mathcal{O}(\lambda^{10})$. Despite Δm_d being currently known with very good precision, the aforementioned theoretical uncertainties limit its effectiveness as a constraint. This is represented graphically in Figure 2.4, which shows the wide allowed region representing the Δm_d constraint. Forming the ratio of the oscillation frequencies as in (2.56) a more powerful constraint may be obtained, which is expressed to leading order as

$$\Delta m_s = \Delta m_d \xi_\Delta^2 \frac{m_{B_s}}{m_{B^0}} \left(\frac{1 - \frac{1}{2}\lambda^2}{\lambda} \right)^2 \frac{1}{(1 - \bar{\rho})^2 + \bar{\eta}^2}. \quad (2.58)$$

Note that while Δm_s has only a weak direct dependence on the parameters $(\bar{\rho}, \bar{\eta})$, neglected in (2.58), it effectively provides a determination of the non-perturbative parameters contained in C_q which enter (2.57). The UT's side R_t (2.51), which corresponds to the circle's radius,

becomes proportional to the inverse of Δm_s . A set of Δm_s values is projected onto the unitarity plane in Figure 2.4. Lower exclusion limits for Δm_s can carry already very useful information, as they impose upper bounds on the magnitude of R_t . A full double-sided measurement of Δm_s will result in a particularly stringent constraint. The power of the latter will also benefit from improvements in the (lattice) calculation of the relevant matrix elements. Conversely, the measurement of Δm_s will effectively provide an “experimental” determination of those hadronic quantities, within the SM framework, which can then be compared against the theoretical predictions.

Other constraints

Several other measurements are used, along with neutral B meson mixing, to over-constrain the UT in a global CKM fit. We briefly mention next some of the most relevant.

The length of the side R_u (2.50) of the UT is constrained from the ratio $|V_{ub}/V_{cb}|$. This is determined from the relative rates of $b \rightarrow ul\bar{\nu}$ and $b \rightarrow cl\bar{\nu}$ decays, and corresponds to a circle centered at the origin in the $(\bar{\rho}, \bar{\eta})$ plane,

$$\bar{\rho}^2 + \bar{\eta}^2 = C_1 . \quad (2.59)$$

The quantities C_i contain both results of experimental measurements and related theoretical computations. From the neutral kaon system, the measurement of indirect CP violation, which is quantified by the asymmetry parameter $|\epsilon_k|$, becomes also useful as the relevant matrix elements can be obtained with accountable, moderate systematic uncertainties. This translates roughly into a hyperbolic constraint of the form

$$\bar{\eta}[1 + C_3(1 - \bar{\rho})] = C_2 . \quad (2.60)$$

The UT angles are all accessible from the B sector, albeit with different sensitivity and purity. The measurements of β and γ are performed through B decays in charmonium and open-charm, respectively, and are theoretically clean, whereas the measurement of α in charmless B decays relies on theoretical assumptions. For the angle β , the leading experimental observable is $\sin 2\beta$, measured from time-dependent CP violation parameters in $b \rightarrow c\bar{c}s$ decays. The measurement of α and γ involve interference with transitions governed by the small CKM matrix element V_{ub} , and require relatively larger data samples. The form of the UT angles’ constraints is encoded in (2.53).

Relative to $\bar{\rho}$ and $\bar{\eta}$, the parameters λ and A are currently measured with a considerably higher precision. The former, λ , is obtained from the magnitude of V_{us} , which is traditionally extracted from semileptonic kaon decays. The latter parameter, A , is determined from $|V_{cb}|$, being most accurately obtained from exclusive and inclusive semileptonic B decays to charm.

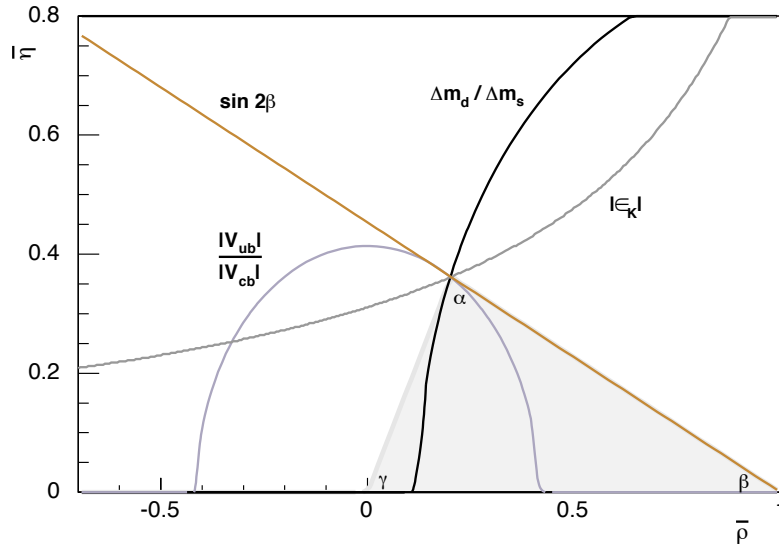


Figure 2.5: Constraints on the unitarity plane, where the compatibility among the observables has been enforced.

A graphical representation of the most relevant constraints, without uncertainties, is exhibited in Figure 2.5; some indicative values for the involved quantities are used while the compatibility between the constraints has been enforced for illustration.

The constraints illustrated in Figure 2.5 may, in reality, turn out to be not all compatible with a single point in the $\bar{\eta}$ - $\bar{\rho}$ space. This is one way in which physics beyond the standard model may be revealed. The realization of the mixing phenomenon within the SM will be now further specified, along with how the parameterization of possible SM deviations may be described.

2.3.2 Standard model relations

While the description presented in Section 2.1 holds rather generally, in the framework of a specific underlying interaction model the relevant matrix elements may be actually computed. In the Standard Model, \mathcal{H}_0 (see (2.2)) accounts for the strong and electromagnetic Hamiltonians, which have stable flavor eigenstates, while $\mathcal{H}_{\Delta F}$ corresponds to the weak interaction perturbation.

In the B systems the off-diagonal matrix elements are given by the leading term

$$M_{12}^q - \frac{i}{2}\Gamma_{12}^q = \langle B_q^0 | \mathcal{H}_{\Delta B=2} | \bar{B}_q^0 \rangle, \quad (2.61)$$

which corresponds to the box diagrams in Figure 2.2 containing internal W and up-type quark

lines. The dispersive (mass) part of the box graph is dominated by the t quark contribution. Its evaluation may be expanded as

$$M_{12}^q = \left(\frac{G_F}{4\pi} \right)^2 (V_{tb}V_{tq}^*)^2 C(\mu) \langle B_q^0 | Q | \bar{B}_q^0 \rangle_{(\mu)}, \quad (2.62)$$

where G_F is the Fermi constant, and V_{ij} denote the CKM matrix elements involved; the factors C and $\langle Q \rangle$ contain respectively the *short distance* (perturbative) and *long distance* (non-perturbative) contributions to the process amplitude, to be evaluated using a consistent renormalization scale μ and scheme.

The Wilson coefficient is given by

$$C(\mu) = m_W^2 S_0 \left(\frac{m_t^2}{m_W^2} \right) \eta_{B_q}(\mu), \quad (2.63)$$

where m_W and m_t are the W boson and top quark masses, respectively, and η_{B_q} is a short distance QCD correction. The Inami-Lim function,

$$S_0(x) = x \left[\frac{1}{4} + \frac{9}{4} \frac{1}{1-x} - \frac{3}{2} \frac{1}{(1-x)^2} \right] - \frac{3}{2} \left[\frac{x}{1-x} \right]^3 \ln x, \quad (2.64)$$

from the loop [95] is approximated well by $0.784x^{0.76}$. An evaluation of $S(m_t^2/m_W^2)$ and η_B within a consistent renormalization scheme yields $S_0 \approx 2.3$, $\eta_B \approx 0.55$.

Integrating out the internal (top quark and W boson) fields from the box diagram leads to a local operator of the form

$$Q = \bar{q} \gamma_\nu (1 - \gamma^5) b \cdot \bar{q} \gamma^\nu (1 - \gamma^5) b. \quad (2.65)$$

The corresponding hadronic matrix element is parameterized as

$$\langle B_q^0 | Q | \bar{B}_q^0 \rangle_{(\mu)} = -\frac{4}{3} m_{B_q} B_{B_q}(\mu) f_{B_q}^2(\mu), \quad (2.66)$$

where m_{B_q} and f_{B_q} are the B_q^0 mass and decay constant, and B_{B_q} is the bag parameter arising from the vacuum insertion approximation. While the scale μ is arbitrary, the physical amplitude (2.62) is independent of both the renormalization scheme and scale.

The absorptive (lifetime) matrix element Γ_{12} involves weak decays common to both B_q^0 and \bar{B}_q^0 . In contrast to the neutral kaon system, these are only a fraction of the B decays. Those states correspond to on-shell, energetically allowed transitions, and thus the top quark loops do not contribute — the leading internal quarks in the box graph are now charm and up quarks which are considerably lighter than the B mesons. It is the latter which here sets the scale, $\Delta\Gamma \propto m_{B_q}$, which, in view of $\Delta m \propto m_t$, supports the inequality $\Delta\Gamma \ll \Delta m$. The

evaluation of the quark box diagram yields in this case

$$\begin{aligned} \Gamma_{12}^q &= -\frac{G_F^2}{8\pi} m_W^2 \eta'_{B_q} m_{B_q} B_{B_q} f_{B_q}^2 [(V_{tq}^* V_{tb})^2 \\ &+ V_{tq}^* V_{tb} V_{cq}^* V_{cb} \mathcal{O}\left(\frac{m_c^2}{m_b^2}\right) + (V_{cq}^* V_{cb})^2 \mathcal{O}\left(\frac{m_c^4}{m_b^4}\right)]. \end{aligned} \quad (2.67)$$

The predicted relationship between the width and mass differences stem from the relations (2.62) and (2.67), along with (2.20) and (2.21). The ratio

$$\left| \frac{\Gamma_{12}}{M_{12}} \right| \simeq \frac{3\pi}{2} \frac{m_b^2}{m_W^2} \frac{1}{S_0(m_t^2/m_W^2)} \sim \mathcal{O}\left(\frac{m_b^2}{m_t^2}\right) \quad (2.68)$$

is approximately independent of CKM elements, and therefore the same for the B^0 and the B_s systems. The width difference may be estimated [10] from

$$\frac{\Delta\Gamma}{\Delta m} \simeq \frac{1}{2} \left| \frac{\Gamma_{12}}{M_{12}} \right| \simeq \mathcal{O}(10^{-3}). \quad (2.69)$$

A large Δm corresponds to a large lifetime difference between the heavy and light states. The fractional width difference for the B_s system is estimated to be $\Delta\Gamma_s/\Gamma_s \simeq (1 \sim 20)\%$, depending on the value of Δm_s .

2.3.3 Parameterization of new physics effects

The presence of new physics may manifest itself in several ways, including incompatibilities of different measurements related to a same SM quantity, significant enhancements of decay rates and asymmetries that are expected to vanish or be very small within the SM, inconsistencies among the values of the angles and/or the sides of the UT, or mixing may be found to differ significantly from SM predictions.

New physics indeed may potentially bring sizable alterations to the standard flavor description. While additional tree-level contributions are in general anticipated to be suppressed in view of existing experimental constraints, large NP contributions may be present in loop-mediated processes where new interactions may play a significant role. This holds in particular for B meson mixing [14].

The existence of new physics may modify the low-energy effective Hamiltonian in several ways. Additional local $\Delta B = 2$ operators may be generated, of the type

$$Q^{NP} \sim \sum \frac{c_{ij}}{\Lambda^2} \bar{q}\Gamma_i b \cdot \bar{q}\Gamma_j b, \quad (2.70)$$

where c_{ij} are the operators' strength and Λ is the NP scale. New contributions to the Wilson coefficients of the SM operators may arise, inducing modifications to the Inami-Lim functions,

$$S_0 \mapsto S_0 + \delta S^{NP}. \quad (2.71)$$

Rather generally, NP may introduce new amplitude contributions to the mixing process, which may be expressed as

$$M_{12}^q = M_{12}^{q,SM} + M_{12}^{q,NP} \quad \text{with} \quad M_{12}^{q,NP} = \langle B_q^0 | \mathcal{H}_{\Delta B=2}^{NP} | \bar{B}_q^0 \rangle. \quad (2.72)$$

General NP models may introduce a large number of new parameters: flavor changing couplings, CP violating phases, short distance coefficients and matrix elements of new local operators. Nevertheless, a mixing process is described by a single amplitude, and can be parameterized, without loss of generality in terms of two parameters which quantify the difference of the complex amplitude with respect to that of the SM. In the presence of NP, the neutral B_q^0 meson oscillation frequency may be parameterized accordingly as

$$\Delta m_q = \Delta m_q^{\text{SM}} |1 + h_q e^{2i\sigma_q}|, \quad (2.73)$$

where Δm_q^{SM} is the SM contribution, and h_q and σ_q denote the relative magnitude and phase of the NP contribution. Inconsistencies with the SM expectations may then be quantified and represented in the (h_q, σ_q) parameter space.

In the case of the B^0 system, the Δm_d and $\sin 2\beta$ constraints may be used to determine h_d and σ_d . The magnitude h_s and the phase σ_s in the B_s system may be correspondingly constrained from measurements of Δm_s and of the angle β_s (2.54). The observable $\sin 2\beta_s$ can be determined from the time-dependent analysis of the CP asymmetry in B_s decays such as $B_s \rightarrow J/\psi \phi$. The effectiveness of such a general, model independent approach will depend on the precision of the experimental measurements, including Δm_s , and on the accuracy of the SM theoretical prediction. The latter has currently sizable uncertainties arising from imprecisely determined CKM factors and hadronic matrix elements.

The ratio of oscillation frequencies $\Delta m_d/\Delta m_s$, as discussed above, is expected to provide a precise determination of the CKM ratio $|V_{td}/V_{ts}|$ within the SM. Remarkably, this remains true in many NP scenarios. In such classes of models, the virtual exchange of new particles in the box diagrams (Figure 2.2) induce modifications to the coefficients C_q in (2.55), namely of the type of (2.71), which cancel in the ratio. This is the case of various classes of NP scenarios, including for instance two-Higgs doublet models and minimal supersymmetry with flavor conservation.

There are large classes of models in which the biggest effects of NP occur in transitions involving the second and the third generations. These leave the flavor-changing transitions between the other families unaffected, thus respecting, in particular, the bounds from kaon physics. The B_s sector is clearly well suited to test such scenarios. The latter comprise certain SUSY GUT models, for example, which predict an enhancement of Δm_s compared to its SM prediction. Another popular scenario, with large effects in flavor physics, involves

Higgs mediated FCNCs in the large $\tan \beta_{\text{SUSY}}$ region ($\tan \beta_{\text{SUSY}}$ is the ratio of the v evs of the two Higgs doublets). Here suppression of Δm_s proportional to $\tan^4 \beta_{\text{SUSY}}$ is predicted [15]. Models with an extra $U(1)'$ gauge boson Z' can induce FCNCs at tree-level if its coupling to physical fermions is non-diagonal. Such Z' bosons often occur, for instance, in the context of GUTs, superstring theories and theories with large extra dimensions.

Some NP scenarios retain the CKM structure. In the so-called minimal flavor violation (MFV) models, the dynamics of flavor violation is completely determined by the structure of the SM Yukawa couplings. In this case, all FCNC and CP violating phenomena are expressed in terms of the CKM matrix and the dominating top quark Yukawa couplings. Several MFV implementations exist in different contexts, including two-Higgs doublet models, supersymmetry, extra dimensions, *etc.* Other models allow noticeably larger modifications. The structure of the CKM matrix is changed, for example, with the addition of a fourth generation, extra singlet quarks, or in Left-Right symmetric models. Sizable Yukawa couplings to the light fermions are favored for instance in scenarios involving leptoquarks and Higgs models with flavor changing couplings.

In general, B_s mixing may receive significant, positive or negative, new physics contributions. Depending on the magnitude of those contributions, and the precision of relevant theoretical computations, various models may be ruled out, or more or less severely constrained, by the experimental determination of Δm_s along with further and improved relevant measurements in the flavor sector.